THE JOURNAL OF PHYSICAL CHEMISTRY C

pubs.acs.org/JPCC Article

Ultrafast Spin Crossover in a Room-Temperature Ferrimagnet: Element-Specific Spin Dynamics in Photoexcited Cobalt Ferrite

Stephen Londo, Somnath Biswas, Jakub Husek, Igor V. Pinchuk, Michael J. Newburger, Alexandra Boyadzhiev, Amanda H. Trout, David W. McComb, Roland Kawakami, and L. Robert Baker*

Cite This: J. Phys. Chem. C 2020, 124, 11368−11375 Read Online

ACCESS | Metrics & More | Article Recommendations | Supporting Information

ABSTRACT: Transition metal complexes capable of photoinduced spin crossover have been widely investigated because of their potential to enable ultrafast optical control of information processing. However, any real application of photoswitchable molecules requires that spin crossover be paired with additional functionality such as long-range magnetic order. Important advances combining these functions are notably reported for a number of bimetallic Prussian Blue analogues; however, to date, PBA-based magnetic photoswitches can only operate below 150 K due to loss of magnetic order. In contrast, cobalt ferrite is a ferrimagnetic semiconductor with a Curie temperature of 790 K and extremely favorable magnetic properties by comparison to state-of-the-art PBAs. The mixed valence electronic structure of cobalt ferrite is reminiscent of cobalt−iron PBA, which is a well-known photoswitch. To investigate the potential for photoswitching in this material, we employ transient XUV spectroscopy to probe charge and spin dynamics with element-specific resolution on the femtosecond time scale. Results show that 400 nm light excites a metal-to-metal charge transfer transition, which drives the crossover of high-spin Co^{2+} to low-spin Co^{3+} with a time constant of 405 ± 29 fs and an internal quantum efficiency of unity. This result establishes the existence of efficient photoswitching in a new class of robust ferrimagnetic spinel ferrites.

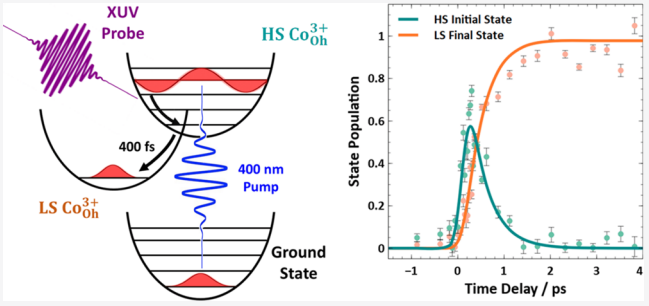

INTRODUCTION

Spin crossover (SCO) materials refer to systems that can change their spin state in response to one or more external stimulus,[1] such as temperature,[2,3] pressure,[4,5] chemical environment,[6−8] or photoexcitation.[9] In particular, photoinduced SCO has been extensively investigated because of its potential for design of ultrafast switches as well as its role in enabling optical control of information processing.[10−12] However, for SCO transitions to be useful, multifunctional materials are needed, which combine photoinduced SCO with another measurable property such as long-range magnetic ordering,[13] electrical conductivity,[14] and/or optical properties (e.g., absorption or fluorescence).[15,16] One of the major current challenges preventing widespread application of SCO materials is the inability to incorporate multifunctionality with spin-state switching under ambient conditions.

For example, Prussian blue analogs (PBAs) represent a promising class of materials, which readily transition between spin states in response to pressure,[17] temperature,[18] and light.[19] Due to the presence of strong electronic exchange coupling across cyano-bridging ligands, these materials display strong metal-to-metal charge transfer absorption bands.[20,21] Excitation of these charge transfer bands have been shown to induce SCO via a mechanism known as charge-transfer-induced spin transition (CTIST).[22,23] Importantly, a number of PBAs also show long-range magnetic ordering. Much work has been done to explore the utility of these materials for ultrafast light-driven magnetic switching. Unfortunately, the magnetic ordering temperature (T_C) of most PBAs is less than 100 K, making them largely impractical for room temperature applications.[24−26]

A few notable exceptions exist, such as mixed valence Cr and V−Cr PBAs. First reported in the mid-90s, these solids display magnetic ordering temperatures approaching or even slightly exceeding room temperature.[27−30] This discovery led to a series of time-resolved optical studies, which showed that the electronic structure of V−Cr PBAs gives rise to charge transfer transitions which drives SCO,[19,27,31] similar to previously studied Fe and Co−Fe analogs. However, follow-up studies focused on improved synthesis of V−Cr PBAs have shown that these materials are often amorphous as well as nonstoichiometric, making it difficult to control the bulk magnetic properties.[30,32]

Received: April 27, 2020
Published: May 4, 2020

https://dx.doi.org/10.1021/acs.jpcc.0c03736
J. Phys. Chem. C 2020, 124, 11368−11375

By comparison, cobalt ferrite (CFO) is a metal oxide semiconductor that belongs to the class of ferrimagnetic spinel ferrites having the general formula MFe_2O_4. In either the normal or inverse crystal structures, Fe is in the 3+ oxidation state and M is a divalent metal cation (e.g., Co^{2+}). CFO has a chemical formula of $[Co_{1-\gamma}^{2+}Fe_{\gamma}^{3+}]_{T_d}[Co_{\gamma}^{2+}Fe_{2-\gamma}^{3+}]_{O_h}O_4$, where γ represents the degree of inversion, indicating that Fe^{3+} and Co^{2+} can exist in both tetrahedral and octahedral sites. In a completely inverse structure, Fe^{3+} occupies all of the tetrahedral sites and half of the octahedral sites and Co^{2+} occupies the remaining half of the octahedral sites. In reality, inversion in this material is not complete with typical inversion parameters on the order of 0.8 (see Supporting Information, Section 2).[33,34] Regardless of the degree of inversion, all metal centers are in the high-spin state with the tetrahedral and octahedral sublattices aligned antiparallel to each other to create ferrimagnetic ordering with a nonvanishing magnetization.

Analysis of the valence structure in CFO reveals that there exists the possibility for photoinduced SCO via a CTIST mechanisms, similar to photoswitching in Co−Fe PBAs.[35] In Co−Fe PBAs, photoexcitation at 660 nm induces electron transfer from Fe^{2+} to Co^{3+} resulting in the ultrafast (<200 fs) photoreduction and subsequent intersystem crossing of LS Co^{3+} to HS Co^{2+}.[36] Unfortunately, Co−Fe PBAs only exhibits photoinduced SCO well below room temperature due to thermal SCO at or above 150 K.[18] Long-range magnetic ordering is even more limited in Co−Fe PBAs having a T_C below 20 K, rendering this material impractical as a room temperature photoswitch.[37]

In contrast, CFO has been shown to have extremely high T_C, saturation magnetization, and coercive field.[38,39] A summary of the magnetic properties of cobalt ferrite compared with state-of-the-art PBAs is summarized in Table 1 and room-temperature magnetic hysteresis measurements of CFO films studied here are provided in the Supporting Information (Section 2) for comparison. In light of these robust magnetic properties, CFO has already been incorporated in a number of spintronic devices as a ferrimagnetic semiconductor for applications including magnetic random access memory,[40] magnetic sensors,[41] and spin filtering via the magnetic proximity effect.[42] However, despite the similar valence structures observed in CFO and Co−Fe PBA, CFO has never been investigated as a SCO material notwithstanding its potentially transformative applications for light activated switching.

Table 1. Comparison of Magnetic and SCO Properties of CFO Thin Films, Co−Fe, and V−Cr PBA Molecular Systems[a]

	Cobalt Ferrite	Co−Fe PBAs	V−Cr PBAs
SCO Time Constant/fs	405 ± 29*	150 to 200[36]†	780[20]
Curie Temperature/K	790[39]	16 to 22[18]	373[19]
Coercive Field/Oe	4.5×10^3 (300 K)[39]	1.5×10^3 (16 K)[25]	5.0×10^1 (5 K)[30]
Saturation Magnetization/cm^3 mol^{-1} G	1.1 to 2.2 × 10^5 (300 K)[39]	6.4×10^3 (16 K)[25]	6.9×10^4 (5 K)[30]
Remanence/%	32 to 35 (300 K)[39]	33 (16 K)[25]	

[a](*) Indicates results from this work while (†) indicates results from simulations.

To investigate the potential SCO dynamics in CFO thin films, we employ ultrafast extreme ultraviolet reflection−absorption (XUV-RA) spectroscopy. Tabletop XUV light sources based on high-harmonic generation have recently extended the benefits of X-ray absorption spectroscopy to probe charge,[43−45] spin,[46−48] and magnetization[49−51] dynamics in materials with ultrafast time resolution. We have developed XUV-RA spectroscopy, a surface-specific analogue of XUV absorption spectroscopy performed in a reflection geometry, to measure ultrafast charge and spin dynamics at surfaces.[52−54] A significant advantage of conducting time-resolved XUV measurements in a reflection compared to traditional transmission geometry is the ability to study extremely high-quality epitaxial samples. With this technique and the findings presented here, we hope to continue the recent efforts that have gone into investigating ultrafast SCO dynamics utilizing X-ray transient absorption spectroscopy.[23,55−57]

RESULTS AND DISCUSSION

To illustrate the nature of the CFO samples measured here, Figure 1a shows a cross-sectional high-angle annular dark-field scanning transmission electron microscopy (HAADF STEM) image of CFO epitaxially grown on magnesium oxide (MgO) substrates. The closely matching lattice parameters of [001] MgO and [001] CFO (0.4% mismatch) gives rise to a highly crystalline film with an atomically sharp interface and cube-on-cube in-plane epitaxial relationship between the film and substrate. The slightly larger lattice constant of MgO produces tensile strain on the CFO film. Figure 1b shows a corresponding AFM image of the CFO samples, confirming that these films are atomically smooth, with a root-mean-square roughness (R_q) of 0.14 nm. RHEED and XPS measurements further confirm the stoichiometry, oxidation states, and crystallinity of these samples, and XPS measurements indicate an inversion parameter of 0.77, which is in agreement with previous reports.[33,34] These data are provided in the Supporting Information (Section 2).

In the present study, XUV-RA spectroscopy is used to simultaneously probe the individual Fe and Co $M_{2,3}$-edge transitions in epitaxial CFO as a function of time delay between the XUV probe (36−72 eV) and 400 nm excitation pulse. Results show that photoexcitation of CFO occurs via a metal-to-metal charge transfer transition, which drives a crossover from high-spin Co^{2+} to low-spin Co^{3+} in 405 ± 29 fs with unity quantum efficiency (100 ± 3.4%). A comparison

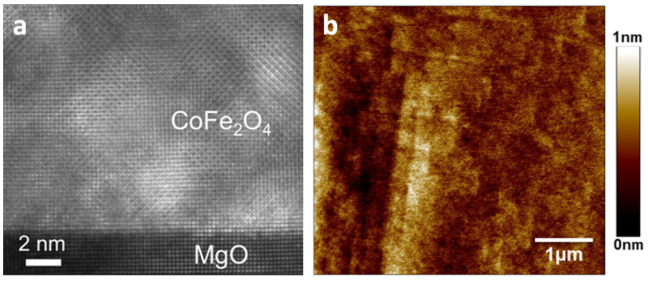

Figure 1. (a) HAADF STEM and (b) AFM measurements demonstrating the highly crystalline nature of the 40 nm CFO thin films.

https://dx.doi.org/10.1021/acs.jpcc.0c03736
J. Phys. Chem. C 2020, 124, 11368−11375

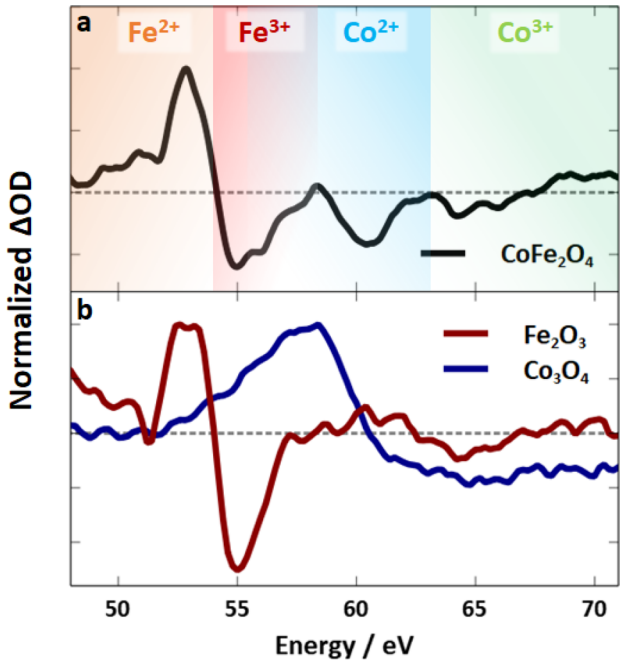

Figure 2. (a) Transient XUV-RA spectra for CFO with different elemental and oxidation states highlighted. (b) Transient XUV-RA spectra for Fe_2O_3 in red and Co_3O_4 in blue.

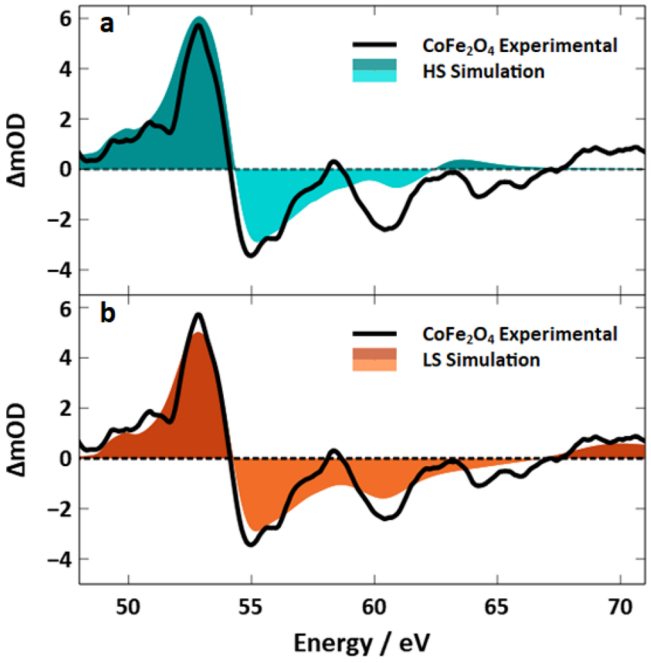

Figure 3. Ligand-field multiplet simulations for (a) HS and (b) LS Co^{3+}. Experimental transient XUV-RA spectrum of CFO is overlaid in black. Excellent agreement is presented between the LS simulation and experimental data, leading to the conclusion of SCO after photoexcitation.

of these results with previous findings for various PBAs is summarized in Table 1. These results establish the existence of efficient, ultrafast photoswitching in this class of robust ferrimagnetic spinel ferrites.

Figure 2a shows the transient XUV-RA spectrum of CFO. Although data was collected for a total of 60 different delay times out to a maximum of 20 ps, this figure shows only the

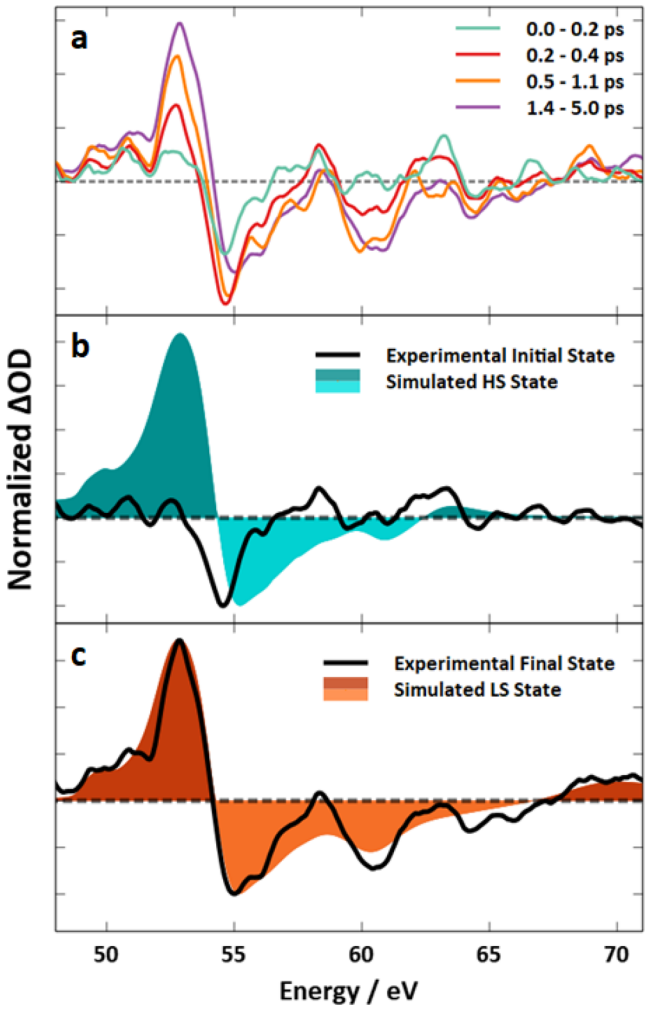

Figure 4. (a) Transient XUV-RA traces for experimental CFO time-averaged for points falling within the ranges listed. Kinetic analysis solutions for the (b) initial and (c) final excited states compared to the HS and LS simulations, respectively. There is good agreement between the final excited state and the LS simulations and qualitative agreement between the initial excited state and HS simulation.

averaged transient spectrum for delay times greater than 400 fs. We find that dramatic spectral evolution occurs during the first several hundred fs, after which the transient spectrum remains relatively constant. The ultrafast spectral evolution occurring on the fs time scale is discussed in detail below. However, here, we first focus on the assignment of the final photoexcited state, which characterizes CFO at times greater than 400 fs following photoexcitation.

Because XUV-RA spectroscopy is sensitive to individual elements and can resolve oxidation and spin states, we are able to comment separately on the final oxidation and spin states of both Fe and Co metal centers. Starting with an oxidation state analysis, this spectrum is able to confirm that photoexcitation in CFO represents a metal-to-metal charge-transfer excitation, where electron density is shifted from Co 3d valence band orbitals to Fe 3d conduction band orbitals. This is observed in the XUV spectrum as a reduction of Fe^{3+} to Fe^{2+} and a corresponding oxidation of Co^{2+} to Co^{3+}. These oxidation state changes are evident by a red shift at the Fe $M_{2,3}$-edge and a blue shift at the Co $M_{2,3}$-edge. Because the transient spectrum shows the difference between the photoexcited state and the

https://dx.doi.org/10.1021/acs.jpcc.0c03736
J. Phys. Chem. C 2020, 124, 11368−11375

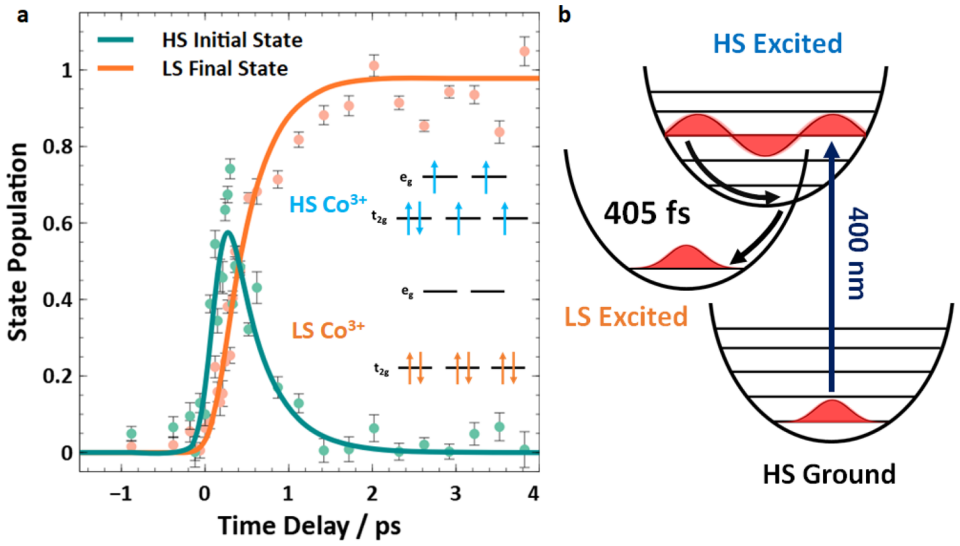

Figure 5. (a) State population for the HS initial and LS final states calculated by the kinetic analysis and the amplitude coefficients from experimental data with standard errors. The inset is a cartoon representation of the change in crystal field splitting which drives the photoinduced SCO. (b) Diagram showing intersystem crossing for CFO thin films. Photoexcitation with 400 nm light excites from the HS Ground to HS Excited state which then relaxes to a LS Excited state with a time constant of 405 ± 29 fs.

ground state, the positive feature represents increased absorption by the excited state, while the negative feature is associated with depopulation of the ground state. Specifically, at the Fe $M_{2,3}$-edge, excited state absorption at 53 eV corresponds to formation of Fe^{2+}, and ground state bleaching at 55 eV corresponds to the depletion of Fe^{3+} ground state. Similarly, at the Co $M_{2,3}$-edge, ground state bleaching at 60.5 eV corresponds to depletion of Co^{2+} and excited state absorption at 69 eV corresponds to formation of Co^{3+}. This analysis indicates the a formation of a charge transfer excited state ($Co^{2+} \rightarrow Fe^{3+}$) in CFO following photoexcitation.

To confirm this assignment, Figure 2 compares the transient spectrum with the results of similar measurements made on monometallic oxides, Fe_2O_3 (red line) and Co_3O_4 (blue line), which both experience a ligand-to-metal charge transfer and subsequent reduction of their respective M^{3+} metal cations (M = Fe or Co) upon photoexcitation.[45,54] In the Fe_2O_3 transient spectrum, this reduction is observed as an excited state absorption by Fe^{2+} at 52.5 eV and a ground state bleach from Fe^{3+} at 55 eV. For Co_3O_4 this reduction is observed as an excited state absorption by Co^{2+} spanning 53−61 eV and a ground state bleach from Co^{3+} spanning 62−70 eV. By comparing the transient features at the Fe and Co $M_{2,3}$-edges of CFO with pure Fe_2O_3 and Co_3O_4, we confirm our assignment of a metal-to-metal charge transfer excited state in CFO. Interestingly, this assignment is different from the ligand-to-metal charge transfer previously observed in closely related spinel Co_3O_4.[45,58] Considering the reason for this distinction, we note that the through-space coupling distance between octahedrally coordinated Co^{2+} and Fe^{3+} centers in the predominately inverse spinel CFO structure is significantly shorter than the distance between Co^{3+} (O_h) and Co^{2+} (T_d) in the normal spinel structure of Co_3O_4. Importantly, this intervalence charge transfer in CFO supports an ultrafast CTIST in this magnetic semiconductor as described below.

To understand the mechanism of the CTIST, we first consider the effect of this metal-to-metal charge-transfer on the equilibrium nuclear configuration in CFO. Reduction of Fe^{3+} to Fe^{2+} will decrease the electrostatic attraction of this metal center with the negatively charged lattice oxygen leading to electron self-trapping via a local bond length expansion around the photoexcited Fe^{2+} center. This process occurs via fast electron−phonon scattering (tens of fs), followed by coupling of the free electron state to an optical phonon to form a small electron polaron (hundreds of fs) and has been studied in detail in α-Fe_2O_3 (hematite).[54,59,60] Here, we observe similar spectral evolution at the Fe $M_{2,3}$-edge occurring on the fs time scale for CFO, indicating that electron polarons also form in this material. By similar logic, oxidation of the Co metal center will increase attraction between photoexcited Co^{3+} and the oxygen anions, leading to bond length contraction and formation of a hole polaron. These have been predicted in materials where valence band carriers localize to metal 3d orbitals.[61,62] Consistent with these predictions, we find that hole density localizes strongly to Co 3d states.[35]

SCO often results from nuclear rearrangements, which occur in response to charge-transfer excitations. These changes in nuclear bond lengths modulate the local crystal field parameters and induce shifts in the *d*-orbital splitting, which lead to CTIST.[48,56,57,63,64] As a rule, a decrease in crystal field splitting (as observed in electron-polaron formation) will favor a low-spin (LS) to high-spin (HS) transition, whereas, an increase in crystal field splitting (as observed in hole-polaron formation) will favor a HS to LS transition. Because Fe and Co metal centers are uniformly HS in the CFO ground state, we would predict no CTIST at the photoexcited Fe center, where electron-polaron formation will serve to further stabilize the native HS configuration. However, a CTIST is predicted at the Co center as hole-polaron formation will increase the crystal field splitting and drive a HS to LS transition on Co^{3+}. This process is closely analogous to photoinduced SCO in molecular Fe and Co complexes which have been shown to occur by vibronic coupling in the excited state manifold leading to intersystem crossing on the time scale of tens to hundreds of fs.[48,65−68] Assuming that a similar process occurs at the surface of CFO, it should be readily detectable in the transient XUV-RA spectrum.

https://dx.doi.org/10.1021/acs.jpcc.0c03736
J. Phys. Chem. C 2020, 124, 11368−11375

To test this hypothesis, we have performed ligand-field multiplet calculations to predict the transient XUV-RA spectra for CFO in both HS and LS configurations.[69] Simulated absorption spectra for $Fe^{2+/3+}$ and $Co^{2+/3+}$ in both octahedral and tetrahedral configurations are summed to obtain a spectrum representing bimetallic CFO, accounting for the 0.77 inversion parameter as measured by XPS. This summed absorption spectrum is then converted into the real and imaginary components of the refractive index to generate a reflection−absorption spectrum. The details of the simulation are provided in the Supporting Information (Section 3).

Given the 0.77 degree of inversion in these samples, there are four distinct $Co^{2+}/Fe^{3+} \rightarrow Co^{3+}/Fe^{2+}$ metal-to-metal charge transfer pathways to consider: (1) $Co_{O_h}{}^{2+}/Fe_{O_h}{}^{3+} \rightarrow Co_{O_h}{}^{3+}/Fe_{O_h}{}^{2+}$, (2) $Co_{O_h}{}^{2+}/Fe_{T_d}{}^{3+} \rightarrow Co_{O_h}{}^{3+}/Fe_{Td}{}^{2+}$, (3) $Co_{T_d}{}^{2+}/Fe_{O_h}{}^{3+} \rightarrow Co_{T_d}{}^{3+}/Fe_{O_h}{}^{2+}$, and (4) $Co_{T_d}{}^{2+}/Fe_{T_d}{}^{3+} \rightarrow Co_{T_d}{}^{3+}/Fe_{T_d}{}^{2+}$. The first two pathways account for possible metal-to-metal charge transfer transitions in the inverse spinel structure. The third pathway accounts for the only analogous transition in the normal spinel structure. The fourth pathway accounts for a transition in the partially inverse structure, which has the possibility of adjacent Co^{2+} and Fe^{3+} T_d centers. Simulations of the transient spectrum for each of these transitions have been considered and are shown in the Supporting Information (Section 3). Comparison of these simulated spectra with the experimental result from Figure 2 indicates that photoexcitation of CFO primarily drives transition (1) above, or in other words, charge transfer between octahedrally coordinated Co^{2+} and Fe^{3+} in the inverse spinel structure. This assignment intuitively agrees well with the crystal structure of CFO: Co and Fe O_h metal centers in the inverse spinel are expected to have the greatest degree of orbital overlap, having a shorter through-space coupling distance of ∼2.8 Å compared to the Co $O_h \rightarrow$ Fe T_d in the inverse spinel or Co $T_d \rightarrow$ Fe O_h in the normal spinel (each ∼3.3 Å) or the Co $T_d \rightarrow$ Fe T_d in the partially inverse structure (∼3.5 Å).

We now consider the effect of charge transfer on the spin state of photoexcited CFO. Figure 3 shows a comparison of the measured transient spectrum for delay times greater than 400 fs with the simulation for a metal-to-metal charge transfer between $Co_{O_h}{}^{2+}$ and $Fe_{Oh}{}^{3+}$. The teal shaded region in Figure 3a represents the predicted spectrum for a metal-to-metal charge-transfer excitation with the Co^{3+} metal center in the native HS configuration, while the orange shaded region in Figure 3b represents the same spectrum with Co^{3+} in the LS configuration. As shown, the experimental spectrum (black line) closely matches the LS simulation, confirming that photoexcitation in CFO drives a CTIST on the ultrafast time scale. Because the excited state spectrum could be a convolution of Co^{3+} in the HS and LS configuration, we define the internal quantum yield for SCO to be the percent of the LS configuration represented in the excited state. To estimate this, simulated spectra for the HS (0% quantum yield) and LS (100% quantum yield) were fit to the experimental excited state spectrum using a nonlinear, least-squares regression in order to determine the ratio of HS and LS Co^{3+} in the excited state. The results show that photoexcited Co^{3+} transitions to the LS spin state with unity probability (100 ± 3.4%), confirming highly efficient intersystem crossing in this material.

To determine the kinetics of photoinduced SCO, Figure 4a shows time-averaged traces of experimental CFO data for the first 200 fs, 200 to 400 fs, 500 to 1.1 ps, and 1.4 to 5 ps following photoexcitation. The ultrafast dynamics of the Fe $M_{2,3}$-edge match well with what has been seen before in Fe_2O_3 and is consistent with ultrafast electron trapping via small polaron formation.[54] Focusing on the Co $M_{2,3}$-edge above approximately 60 eV immediately after photoexcitation, the spectrum is characterized by a weak excited state absorption at 63 eV. During the subsequent several hundred fs, a ground state bleach forms at 60 eV and the excited state absorption is shifted to higher energy at 68 eV.

To quantify this spectral evolution, we utilize a global fitting analysis package which models the spectral evolution of the experimental data as two, sequentially evolving 1st-order kinetic components convoluted with a Gaussian instrument response function.[70] The solutions to these equations are spectrally resolved as the initial and final excited states for photoexcited CFO. Figure 4b,c shows these initial and final state solutions (black lines) with the HS and LS simulations shaded in teal and orange, respectively. We note that the final state closely matches the simulated spectrum for LS Co^{3+} consistent with a CTIST on photoexcited Co^{3+}. In contrast, the initial state qualitatively matches the simulated spectrum for HS Co^{3+} in the Co $M_{2,3}$-edge spectral region. From these results, we propose that the spectral evolution at the Co $M_{2,3}$-edge represents the conversion of HS Co^{3+} to LS Co^{3+} on the ultrafast time scale following photoexcitation. We note that the initial state spectrum does not show an exact fit to the results of ligand-field multiplet calculations at the Fe $M_{2,3}$-edge. This discrepancy has been reported previously for α-Fe_2O_3 and is related to ultrafast electron trapping at the oxide surface via small polaron formation, which is occurring simultaneously with SCO.[54]

The time constant for this spectral evolution is obtained from the global kinetic analysis and is depicted in Figure 5a. Amplitude coefficients of each state are obtained from experimental spectra as a function of time delay using a multivariate regression analysis and are shown along with standard errors overlaying the global kinetic analysis traces. The HS state converts to a LS state, eventually reaching a steady population following 2 ps. The first order time constant for SCO obtained from this analysis is 405 ± 29 fs. This time constant for intersystem crossing is similar to what has been previously reported for CTIST in a variety of PBA systems[20,36] and a schematic of this process is depicted in Figure 5b. Ground state CFO is in the HS configuration for both Fe and Co metal centers. After photoexcitation with 400 nm light, the system is driven into a HS Co^{3+} excited state which then relaxes into a LS excited state via intersystem crossing. No evidence of excited state relaxation is observed out to 20 ps, which is the longest time delay investigated in this study, and additional work will be required to quantify the exact relaxation lifetime of the LS Co^{3+} excited state.

We note that an important remaining question is the effect of this CTIST on the long-range magnetic ordering in photoexcited CFO. We expect that in this ferrimagnet, where the nonvanishing magnetic moment comes from alignment of HS Co^{2+} centers, the bulk magnetism will be strongly modulated by the observed HS to LS transition, which occurs with unity efficiency on photoexcited Co^{3+}. Similarly, while O_h and T_d Fe^{3+} centers antiferromagnetically align in the ground state of CFO, transfer of an additional electron to O_h sites may

https://dx.doi.org/10.1021/acs.jpcc.0c03736
J. Phys. Chem. C 2020, 124, 11368−11375

create a transient, nonvanishing magnetic moment on Fe centers depending on the nature of the excited state exchange interactions. These questions are beyond the scope of the present study, where XUV-RA only probes the local spin configuration of photoexcited CFO but is insensitive to net magnetic ordering. We hope to address these questions in the near future using XUV circular dichroism measurements, which have been used to study magnetic transitions on the ultrafast time scale.[71,72]

CONCLUSION

Here, we present the first investigation of photoinduced spin dynamics in CFO. Ultrafast XUV-RA measurements show the element-specific oxidation and spin-state dynamics in this material on the femtosecond time scale. Spectral analysis demonstrates that photoexcitation of CFO at 400 nm excites a metal-to-metal charge transfer transition that drives intersystem crossing from HS Co^{2+} to LS Co^{3+} via a CTIST mechanism. This process occurs with a time constant of 405 ± 29 fs and unity quantum efficiency. SCO in this material is enabled by the presence of an intervalence charge transfer transition. We hypothesize that this intervalence transition, which is unique to CFO compared to Co_3O_4, is facilitated by the stronger metal−metal coupling in the predominately inverse spinel structure of CFO. This observation indicates that other magnetic materials in this class of ferrimagnetic inverse spinel ferrites are also expected to support efficient photoinduced SCO.

Photoinduced SCO has potential to enable ultrafast, optical control of information storage and processing. However, this requires that SCO be paired with additional material functionality such as long-range magnetic order. PBAs have been extensively investigated as potential photoswitches due to their combination of ultrafast SCO and ferromagnetic ordering. Unfortunately, applications are generally limited due to poor magnetic properties and/or the loss of magnetic ordering far below room temperature. In contrast, CFO has a T_C of 790 K and extremely favorable magnetic properties by comparison to state-of-the-art PBAs. Consequently, this finding establishes the existence of efficient photoinduced SCO in a robust ferrimagnetic semiconductor, which is a necessary step to enable a variety of spintronic applications requiring room temperature photoswitching.

ASSOCIATED CONTENT

Supporting Information

The Supporting Information is available free of charge at https://pubs.acs.org/doi/10.1021/acs.jpcc.0c03736.

Sample preparation, details of transient XUV-RA spectroscopy, sample characterization, and details of ligand field multiplet simulations (PDF)

AUTHOR INFORMATION

Corresponding Author

L. Robert Baker − *Department of Chemistry and Biochemistry, The Ohio State University, Columbus, Ohio 43210, United States;* orcid.org/0000-0001-6740-864X; Email: baker.2364@osu.edu

Authors

Stephen Londo − *Department of Chemistry and Biochemistry, The Ohio State University, Columbus, Ohio 43210, United States;* orcid.org/0000-0002-6456-9680

Somnath Biswas − *Department of Chemistry and Biochemistry, The Ohio State University, Columbus, Ohio 43210, United States;* orcid.org/0000-0002-5931-4966

Jakub Husek − *Department of Chemistry and Biochemistry, The Ohio State University, Columbus, Ohio 43210, United States;* orcid.org/0000-0003-4820-462X

Igor V. Pinchuk − *Department of Physics, The Ohio State University, Columbus, Ohio 43210, United States*

Michael J. Newburger − *Department of Physics, The Ohio State University, Columbus, Ohio 43210, United States*

Alexandra Boyadzhiev − *Department of Physics, The Ohio State University, Columbus, Ohio 43210, United States*

Amanda H. Trout − *Department of Materials Science and Engineering and USA Center for Electron Microscopy and Analysis, The Ohio State University, Columbus, Ohio 43210, United States*

David W. McComb − *Department of Materials Science and Engineering and USA Center for Electron Microscopy and Analysis, The Ohio State University, Columbus, Ohio 43210, United States*

Roland Kawakami − *Department of Physics, The Ohio State University, Columbus, Ohio 43210, United States;* orcid.org/0000-0003-0245-9192

Complete contact information is available at: https://pubs.acs.org/10.1021/acs.jpcc.0c03736

Notes

The authors declare no competing financial interest.

ACKNOWLEDGMENTS

XUV measurements and spectral simulations were supported by Chemical Sciences, Geosciences and Biosciences Division, Office of Basic Energy Sciences, Office of Sciences, U.S. Department of Energy under DOE award number DE-SC0014051. Growth and characterization of CFO thin films was supported by the Center for Emergent Materials: an NSF MRSEC under award number DMR-1420451. HAADF-STEM imaging was performed at the OSU Center for Electron Microscopy and Analysis.

REFERENCES

(1) Halcrow, M. A. *Spin-crossover materials: properties and applications*; John Wiley & Sons: 2013.

(2) Shepherd, H. J.; Molnár, G.; Nicolazzi, W.; Salmon, L.; Bousseksou, A. Spin crossover at the nanometre scale. *Eur. J. Inorg. Chem.* **2013**, *2013*, 653−661.

(3) Bernien, M.; Naggert, H.; Arruda, L. M.; Kipgen, L.; Nickel, F.; Miguel, J.; Hermanns, C. F.; Krüger, A.; Krüger, D.; Schierle, E.; et al. Highly efficient thermal and light-induced spin-state switching of an Fe (II) complex in direct contact with a solid surface. *ACS Nano* **2015**, *9*, 8960−8966.

(4) Cowan, M. G.; Olguín, J.; Narayanaswamy, S.; Tallon, J. L.; Brooker, S. Reversible switching of a cobalt complex by thermal, pressure, and electrochemical stimuli: abrupt, complete, hysteretic spin crossover. *J. Am. Chem. Soc.* **2012**, *134*, 2892−2894.

(5) Antonangeli, D.; Siebert, J.; Aracne, C. M.; Farber, D. L.; Bosak, A.; Hoesch, M.; Krisch, M.; Ryerson, F. J.; Fiquet, G.; Badro, J. Spin crossover in ferropericlase at high pressure: A seismologically transparent transition? *Science* **2011**, *331*, 64−67.

(6) Halder, G. J.; Kepert, C. J.; Moubaraki, B.; Murray, K. S.; Cashion, J. D. Guest-dependent spin crossover in a nanoporous molecular framework material. *Science* **2002**, *298*, 1762−1765.
(7) Boskovic, C.; Brechin, E. K.; Streib, W. E.; Folting, K.; Bollinger, J. C.; Hendrickson, D. N.; Christou, G. Single-molecule magnets: a new family of Mn12 clusters of formula [Mn12O8 × 4 (O2CPh) 8L6]. *J. Am. Chem. Soc.* **2002**, *124*, 3725−3736.
(8) Wu, D.-Q.; Shao, D.; Wei, X.-Q.; Shen, F.-X.; Shi, L.; Kempe, D.; Zhang, Y.-Z.; Dunbar, K. R.; Wang, X.-Y. Reversible On−Off Switching of a Single-Molecule Magnet via a Crystal-to-Crystal Chemical Transformation. *J. Am. Chem. Soc.* **2017**, *139*, 11714−11717.
(9) Ohkoshi, S.-i.; Imoto, K.; Tsunobuchi, Y.; Takano, S.; Tokoro, H. Light-induced spin-crossover magnet. *Nat. Chem.* **2011**, *3*, 564.
(10) Kimble, H. J. The quantum internet. *Nature* **2008**, *453*, 1023.
(11) Raman, K. V.; Kamerbeek, A. M.; Mukherjee, A.; Atodiresei, N.; Sen, T. K.; Lazić, P.; Caciuc, V.; Michel, R.; Stalke, D.; Mandal, S. K.; et al. Interface-engineered templates for molecular spin memory devices. *Nature* **2013**, *493*, 509.
(12) Tiecke, T.; Thompson, J. D.; de Leon, N. P.; Liu, L.; Vuletić, V.; Lukin, M. D. Nanophotonic quantum phase switch with a single atom. *Nature* **2014**, *508*, 241.
(13) Barskaya, I. Y.; Tretyakov, E. V.; Sagdeev, R. Z.; Ovcharenko, V. I.; Bagryanskaya, E. G.; Maryunina, K. Y.; Takui, T.; Sato, K.; Fedin, M. V. Photoswitching of a thermally unswitchable molecular magnet cu (hfac) 2li-pr evidenced by steady-state and time-resolved electron paramagnetic resonance. *J. Am. Chem. Soc.* **2014**, *136*, 10132−10138.
(14) Suda, M.; Kato, R.; Yamamoto, H. M. Light-induced superconductivity using a photoactive electric double layer. *Science* **2015**, *347*, 743−746.
(15) Lochenie, C.; Schötz, K.; Panzer, F.; Kurz, H.; Maier, B.; Puchtler, F.; Agarwal, S.; Köhler, A.; Weber, B. Spin-crossover iron (II) coordination polymer with fluorescent properties: Correlation between emission properties and spin state. *J. Am. Chem. Soc.* **2018**, *140*, 700−709.
(16) Benaicha, B.; Van Do, K.; Yangui, A.; Pittala, N.; Lusson, A.; Sy, M.; Bouchez, G.; Fourati, H.; Gómez-García, C. J.; Triki, S. Interplay between spin-crossover and luminescence in a multifunctional single crystal iron (ii) complex: towards a new generation of molecular sensors. *Chemical Science* **2019**, *10*, 6791.
(17) Pinkowicz, D.; Rams, M.; Misek, M.; Kamenev, K. V.; Tomkowiak, H.; Katrusiak, A.; Sieklucka, B. Enforcing multifunctionality: a pressure-induced spin-crossover photomagnet. *J. Am. Chem. Soc.* **2015**, *137*, 8795−8802.
(18) Aguila, D.; Prado, Y.; Koumousi, E. S.; Mathoniere, C.; Clérac, R. Switchable Fe/Co Prussian blue networks and molecular analogues. *Chem. Soc. Rev.* **2016**, *45*, 203−224.
(19) Bozdag, K. D.; Yoo, J.-W.; Raju, N.; McConnell, A. C.; Miller, J. S.; Epstein, A. Optical control of magnetization in a room-temperature magnet: V-Cr Prussian blue analog. *Phys. Rev. B: Condens. Matter Mater. Phys.* **2010**, *82*, 094449.
(20) Johansson, J.; Kim, J.-W.; Allwright, E.; Rogers, D.; Robertson, N.; Bigot, J.-Y. Directly probing spin dynamics in a molecular magnet with femtosecond time-resolution. *Chemical science* **2016**, *7*, 7061−7067.
(21) Koumousi, E. S.; Jeon, I.-R.; Gao, Q.; Dechambenoit, P.; Woodruff, D. N.; Merzeau, P.; Buisson, L.; Jia, X.; Li, D.; Volatron, F.; et al. Metal-to-metal electron transfer in Co/Fe Prussian blue molecular analogues: the ultimate miniaturization. *J. Am. Chem. Soc.* **2014**, *136*, 15461−15464.
(22) Shimamoto, N.; Ohkoshi, S.-i.; Sato, O.; Hashimoto, K. Control of charge-transfer-induced spin transition temperature on cobalt- iron prussian blue analogues. *Inorg. Chem.* **2002**, *41*, 678−684.
(23) Zerdane, S.; Cammarata, M.; Balducci, L.; Bertoni, R.; Catala, L.; Mazerat, S.; Mallah, T.; Pedersen, M. N.; Wulff, M.; Nakagawa, K.; et al. Probing Transient Photoinduced Charge Transfer in Prussian Blue Analogues with Time-Resolved XANES and Optical Spectroscopy. *Eur. J. Inorg. Chem.* **2018**, *2018*, 272−277.
(24) Bhatt, P.; Bhatt, R.; Mukadam, M.; Yusuf, S. Prussian blue based molecular magnet K 0.3 Mn 2.85 [Cr (CN) 6] 2 n H 2 O with ferrimagnetic ordering temperature of 60 K. *AIP Conf. Proc.* **2012**, 1082−1083.
(25) Sato, O.; Iyoda, T.; Fujishima, A.; Hashimoto, K. Photoinduced magnetization of a cobalt-iron cyanide. *Science* **1996**, *272*, 704−705.
(26) Herren, F.; Fischer, P.; Ludi, A.; Hälg, W. Neutron diffraction study of Prussian Blue, Fe4 [Fe (CN) 6] 3. xH2O. Location of water molecules and long-range magnetic order. *Inorg. Chem.* **1980**, *19*, 956−959.
(27) Ferlay, S.; Mallah, T.; Ouahes, R.; Veillet, P.; Verdaguer, M. A room-temperature organometallic magnet based on Prussian blue. *Nature* **1995**, *378*, 701−703.
(28) Mallah, T.; Thiébaut, S.; Verdaguer, M.; Veillet, P. High-Tc molecular-based magnets: ferrimagnetic mixed-valence chromium (III)-chromium (II) cyanides with Tc at 240 and 190 K. *Science* **1993**, *262*, 1554−1557.
(29) Manriquez, J. M.; Yee, G. T.; McLean, R. S.; Epstein, A. J.; Miller, J. S. A room-temperature molecular/organic-based magnet. *Science* **1991**, *252*, 1415−1417.
(30) Garde, R.; Villain, F.; Verdaguer, M. Molecule-based room-temperature magnets: catalytic role of V (III) in the synthesis of vanadium- chromium Prussian blue analogues. *J. Am. Chem. Soc.* **2002**, *124*, 10531−10538.
(31) Holmes, S. M.; Girolami, G. S. Sol- Gel Synthesis of KVII [CrIII (CN) 6] 2H2O: A Crystalline Molecule-Based Magnet with a Magnetic Ordering Temperature above 100 C. *J. Am. Chem. Soc.* **1999**, *121*, 5593−5594.
(32) Garde, R.; Herrera, J. M.; Villain, F.; Verdaguer, M. Molecule-based magnets with TC above room temperature: Improved synthesis of vanadium−chromium Prussian blue analogues with inserted alkali cations. *Inorg. Chim. Acta* **2008**, *361*, 3597−3602.
(33) Carta, D.; Casula, M. F.; Falqui, A.; Loche, D.; Mountjoy, G.; Sangregorio, C.; Corrias, A. A structural and magnetic investigation of the inversion degree in ferrite nanocrystals MFe2O4 (M= Mn, Co, Ni). *J. Phys. Chem. C* **2009**, *113*, 8606−8615.
(34) De Santis, M.; Bailly, A.; Coates, I.; Grenier, S.; Heckmann, O.; Hricovini, K.; Joly, Y.; Langlais, V.; Ramos, A. Y.; Richter, C. Epitaxial growth and structure of cobalt ferrite thin films with large inversion parameter on Ag (001). *Acta Crystallogr., Sect. B: Struct. Sci., Cryst. Eng. Mater.* **2019**, *75*, 8.
(35) Dileep, K.; Loukya, B.; Pachauri, N.; Gupta, A.; Datta, R. Probing optical band gaps at the nanoscale in NiFe2O4 and CoFe2O4 epitaxial films by high resolution electron energy loss spectroscopy. *J. Appl. Phys.* **2014**, *116*, 103505.
(36) van Veenendaal, M. Ultrafast intersystem crossings in Fe-Co Prussian blue analogues. *Sci. Rep.* **2017**, *7*, 6672.
(37) Avendano, C.; Hilfiger, M. G.; Prosvirin, A.; Sanders, C.; Stepien, D.; Dunbar, K. R. Temperature and light induced bistability in a Co3 [Os (CN) 6] 2 6H2O Prussian blue analog. *J. Am. Chem. Soc.* **2010**, *132*, 13123−13125.
(38) Matzen, S.; Moussy, J.-B.; Mattana, R.; Petroff, F.; Gatel, C.; Warot-Fonrose, B.; Cezar, J.; Barbier, A.; Arrio, M.-A.; Sainctavit, P. Restoration of bulk magnetic properties by strain engineering in epitaxial CoFe2O4 (001) ultrathin films. *Appl. Phys. Lett.* **2011**, *99*, 052514.
(39) Eskandari, F.; Porter, S.; Venkatesan, M.; Kameli, P.; Rode, K.; Coey, J. Magnetization and anisotropy of cobalt ferrite thin films. *Physical Review Materials* **2017**, *1*, 074413.
(40) Mahbub, A. R.; Haque, A.; Ghosh, K. Fabrication and Magnetic Characterization of CFO/NiO and CFO/NiS Heterostructures. *J. Supercond. Novel Magn.* **2019**, *1*−*8*, 2857.
(41) Kakade, S. G.; Ma, Y.-R.; Devan, R. S.; Kolekar, Y. D.; Ramana, C. V. Dielectric, Complex Impedance, and Electrical Transport Properties of Erbium (Er3+) Ion-Substituted Nanocrystalline, Cobalt-Rich Ferrite (Co1. 1Fe1. 9−x Er x O4). *J. Phys. Chem. C* **2016**, *120*, 5682−5693.
(42) Amamou, W.; Pinchuk, I. V.; Trout, A. H.; Williams, R. E.; Antolin, N.; Goad, A.; O'Hara, D. J.; Ahmed, A. S.; Windl, W.;

McComb, D. W.; et al. Magnetic proximity effect in Pt/CoFe 2 O 4 bilayers. *Physical Review Materials* **2018**, *2*, 011401.
(43) Vura-Weis, J.; Jiang, C.-M.; Liu, C.; Gao, H.; Lucas, J. M.; de Groot, F. M.; Yang, P.; Alivisatos, A. P.; Leone, S. R. Femtosecond M2, 3-edge spectroscopy of transition-metal oxides: photoinduced oxidation state change in α-Fe2O3. *J. Phys. Chem. Lett.* **2013**, *4*, 3667−3671.
(44) Baker, L. R.; Jiang, C.-M.; Kelly, S. T.; Lucas, J. M.; Vura-Weis, J.; Gilles, M. K.; Alivisatos, A. P.; Leone, S. R. Charge carrier dynamics of photoexcited Co3O4 in methanol: extending high harmonic transient absorption spectroscopy to liquid environments. *Nano Lett.* **2014**, *14*, 5883−5890.
(45) Jiang, C.-M.; Baker, L. R.; Lucas, J. M.; Vura-Weis, J.; Alivisatos, A. P.; Leone, S. R. Characterization of photo-induced charge transfer and hot carrier relaxation pathways in spinel cobalt oxide (Co3O4). *J. Phys. Chem. C* **2014**, *118*, 22774−22784.
(46) Siegrist, F.; Gessner, J. A.; Ossiander, M.; Denker, C.; Chang, Y.-P.; Schröder, M. C.; Guggenmos, A.; Cui, Y.; Walowski, J.; Martens, U. Light-wave dynamic control of magnetism. *Nature* **2019**, *571*, 240.
(47) Ryland, E. S.; Lin, M.-F.; Verkamp, M. A.; Zhang, K.; Benke, K.; Carlson, M.; Vura-Weis, J. Tabletop Femtosecond M-edge X-ray Absorption Near-Edge Structure of FeTPPCl: Metalloporphyrin Photophysics from the Perspective of the Metal. *J. Am. Chem. Soc.* **2018**, *140*, 4691−4696.
(48) Zhang, K.; Ash, R.; Girolami, G.; Vura-Weis, J. Tracking the Metal-Centered Triplet in Photoinduced Spin Crossover of Fe (phen) 32+ with Tabletop Femtosecond M-Edge X-ray Absorption Near-Edge Structure Spectroscopy. *J. Am. Chem. Soc.* **2019**, *141*, 17180−17188.
(49) Tengdin, P.; You, W.; Chen, C.; Shi, X.; Zusin, D.; Zhang, Y.; Gentry, C.; Blonsky, A.; Keller, M.; Oppeneer, P. M.; et al. Critical behavior within 20 fs drives the out-of-equilibrium laser-induced magnetic phase transition in nickel. *Science advances* **2018**, *4*, No. eaap9744.
(50) Willems, F.; Smeenk, C.; Zhavoronkov, N.; Kornilov, O.; Radu, I.; Schmidbauer, M.; Hanke, M.; von Korff Schmising, C.; Vrakking, M.; Eisebitt, S. Probing ultrafast spin dynamics with high-harmonic magnetic circular dichroism spectroscopy. *Phys. Rev. B: Condens. Matter Mater. Phys.* **2015**, *92*, 220405.
(51) Willems, F.; Sharma, S.; Schmising, C. v. K.; Dewhurst, J.; Salemi, L.; Schick, D.; Hessing, P.; Strüber, C.; Engel, W.; Eisebitt, S. Magneto-Optical Functions at the 3 p Resonances of Fe, Co, and Ni: Ab initio Description and Experiment. *Phys. Rev. Lett.* **2019**, *122*, 217202.
(52) Cirri, A.; Husek, J.; Biswas, S.; Baker, L. R. Achieving Surface Sensitivity in Ultrafast XUV Spectroscopy: M2, 3-Edge Reflection−Absorption of Transition Metal Oxides. *J. Phys. Chem. C* **2017**, *121*, 15861−15869.
(53) Biswas, S.; Husek, J.; Baker, L. R. Elucidating ultrafast electron dynamics at surfaces using extreme ultraviolet (XUV) reflection−absorption spectroscopy. *Chem. Commun.* **2018**, *54*, 4216−4230.
(54) Husek, J.; Cirri, A.; Biswas, S.; Baker, L. R. Surface electron dynamics in hematite (α-Fe2O3): correlation between ultrafast surface electron trapping and small polaron formation. *Chemical science* **2017**, *8*, 8170−8178.
(55) Brossard, S.; Volatron, F.; Lisnard, L.; Arrio, M.-A.; Catala, L.; Mathonière, C.; Mallah, T.; Cartier dit Moulin, C.; Rogalev, A.; Wilhelm, F.; et al. Investigation of the photoinduced magnetization of Copper octacyanomolybdates nanoparticles by X-ray Magnetic Circular Dichroism. *J. Am. Chem. Soc.* **2012**, *134*, 222−228.
(56) Lemke, H. T.; Kjær, K. S.; Hartsock, R.; Van Driel, T. B.; Chollet, M.; Glownia, J. M.; Song, S.; Zhu, D.; Pace, E.; Matar, S. F.; et al. Coherent structural trapping through wave packet dispersion during photoinduced spin state switching. *Nat. Commun.* **2017**, *8*, 1−8.
(57) Kjær, K. S.; Van Driel, T. B.; Harlang, T. C.; Kunnus, K.; Biasin, E.; Ledbetter, K.; Hartsock, R. W.; Reinhard, M. E.; Koroidov, S.; Li, L.; et al. Finding intersections between electronic excited state potential energy surfaces with simultaneous ultrafast X-ray scattering and spectroscopy. *Chemical science* **2019**, *10*, 5749−5760.
(58) Biswas, S.; Husek, J.; Londo, S.; Baker, L. R. Highly localized charge transfer excitons in metal oxide semiconductors. *Nano Lett.* **2018**, *18*, 1228−1233.
(59) Carneiro, L. M.; Cushing, S. K.; Liu, C.; Su, Y.; Yang, P.; Alivisatos, A. P.; Leone, S. R. Excitation-wavelength-dependent small polaron trapping of photoexcited carriers in α-Fe 2 O 3. *Nat. Mater.* **2017**, *16*, 819.
(60) Biswas, S.; Wallentine, S.; Bandaranayake, S.; Baker, L. R. Controlling polaron formation at hematite surfaces by molecular functionalization probed by XUV reflection-absorption spectroscopy. *J. Chem. Phys.* **2019**, *151*, 104701.
(61) Hoang, K. Polaron formation, native defects, and electronic conduction in metal tungstates. *Physical Review Materials* **2017**, *1*, 024603.
(62) Hoang, K.; Oh, M.; Choi, Y. Electronic structure, polaron formation, and functional properties in transition-metal tungstates. *RSC Adv.* **2018**, *8*, 4191−4196.
(63) Zhang, W.; Alonso-Mori, R.; Bergmann, U.; Bressler, C.; Chollet, M.; Galler, A.; Gawelda, W.; Hadt, R. G.; Hartsock, R. W.; Kroll, T.; et al. Tracking excited-state charge and spin dynamics in iron coordination complexes. *Nature* **2014**, *509*, 345−348.
(64) Bertoni, R.; Cammarata, M.; Lorenc, M.; Matar, S. F.; Létard, J.-F.; Lemke, H. T.; Collet, E. Ultrafast light-induced spin-state trapping photophysics investigated in Fe (phen) 2 (NCS) 2 spin-crossover crystal. *Acc. Chem. Res.* **2015**, *48*, 774−781.
(65) Hauser, A. *Spin crossover in transition metal compounds II*; Springer: 2004; pp 155−198.
(66) Marino, A.; Chakraborty, P.; Servol, M.; Lorenc, M.; Collet, E.; Hauser, A. The Role of Ligand-Field States in the Ultrafast Photophysical Cycle of the Prototypical Iron (II) Spin-Crossover Compound [Fe (ptz) 6](BF4) 2. *Angew. Chem., Int. Ed.* **2014**, *53*, 3863−3867.
(67) Ould-Hamouda, A.; Viquerat, B.; Degert, J.; Matar, S. F.; Létard, J. F.; Guillaume, F.; Freysz, E. Impact of Spin State Transition on Vibrations of [Fe−(PM−BiA) 2 (NCS) 2] and [Fe−(PM−PEA) 2 (NCS) 2] Spin Crossover Compounds: Experimental and Theoretical Far IR and Raman Study. *Eur. J. Inorg. Chem.* **2018**, *2018*, 385−393.
(68) Molnár, G.; Mikolasek, M.; Ridier, K.; Fahs, A.; Nicolazzi, W.; Bousseksou, A. Molecular Spin Crossover Materials: Review of the Lattice Dynamical Properties. *Ann. Phys.* **2019**, *531*, 1900076.
(69) Stavitski, E.; De Groot, F. M. The CTM4XAS program for EELS and XAS spectral shape analysis of transition metal L edges. *Micron* **2010**, *41*, 687−694.
(70) Snellenburg, J.; Laptenok, S.; Seger, R.; Mullen, K.; Van Stokkum, I. *Glotaran: A Java-based graphical user interface for the R package TIMP*. 2012,.
(71) Fan, T.; Grychtol, P.; Knut, R.; Hernández-García, C.; Hickstein, D. D.; Zusin, D.; Gentry, C.; Dollar, F. J.; Mancuso, C. A.; Hogle, C. W.; et al. Bright circularly polarized soft X-ray high harmonics for X-ray magnetic circular dichroism. *Proc. Natl. Acad. Sci. U. S. A.* **2015**, *112*, 14206−14211.
(72) Dewhurst, J.; Willems, F.; Elliott, P.; Li, Q.; von Korff Schmising, C.; Strüber, C.; Engel, D.; Eisebitt, S.; Sharma, S. Element Specificity of Transient Extreme Ultraviolet Magnetic Dichroism. *Phys. Rev. Lett.* **2020**, *124*, 077203.

https://dx.doi.org/10.1021/acs.jpcc.0c03736
J. Phys. Chem. C 2020, 124, 11368−11375